Electronic Supplementary Material (ESI) for Journal of Materials Chemistry A.

An energy-saving, bending sensitive, and self-healing PVA-borax-IL ternary hydrogel electrolyte for visual flexible electrochromic strain sensors

Jia-ning Liu, Qi He, Ming-yue Pan, Kui Du, Cheng-Bin Gong and Qian Tang**

S1. Instruments

Fourier-transform infrared (FT-IR) spectra were recorded on a BRUKER TENSOR 27010409 FT-IR spectrometer in the transmittance mode with spectral range of 4000−400 cm^{-1} and a resolution of 2 cm^{-1} by KBr pellets. X-ray diffraction (XRD) patterns were recorded on a XD-6 (Beijing Purkinje General Instrument Co., Ltd, P. R. China) using nickel filtered Cu Kα radiation (λ = 1.5406 Å) and operating at 36 kV and 20 mA over the 2θ range of 5−35° with a scanning speed of 1° min^{-1} and a step size of 0.05° at ambient temperature. The freezing point of hydrogels were characterized by differential scanning calorimetry (PerkinElmer, DSC 4000). Samples were measured under a flow of nitrogen flow at 40 μL min^{-1} and cooled down from 25 ℃ to −50 ℃ at a rate of 5 ℃ min^{-1}. After equilibrating at −50 ℃ for 30 min, the samples were then heated up to 25 ℃ at a rate of 1 ℃ min^{-1}. The linear sweep voltammetry was performed on CHI660B with a sweep rate of 0.1 V s^{-1} and a voltage operating window range of 0−6 V. The HGE samples with a thickness of 0.5 mm was clamped between two stainless steel electrodes to assemble a button battery. Ultraviolet–visible (UV–vis) spectra and electrochromic performance of AVCOOEt-based hydrogel-state ECDs were performed by combining a Shimadzu UV-2700 spectrophotometer at the wavelength from 300–800 nm and RST5060F electrochemical workstation. The color state of the AVCOOEt-based ECDs were recorded by measuring the CIE (International Commission on illumination) L*a*b* color space coordinates with a color reader CR-10 plus (Konica Minolta, Inc., Japan) under electrochemical control. The morphological structures of the freeze-dried hydrogel films coated with gold were investigated by scanning electron microscopy (SEM, Hitachi TM-3030, Japan) at an acceleration voltage of 10.0 kV.

S2. Synthesis of AVCOOEt

Scheme 1 depicts the synthetic procedure for AVCOOEt.

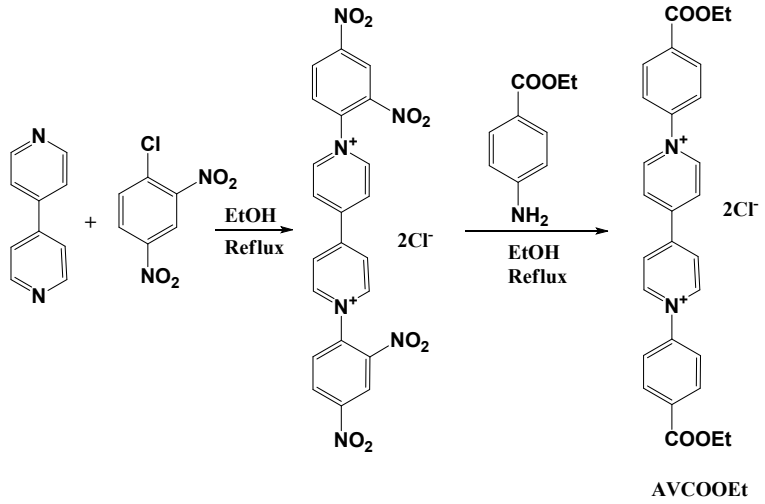

Scheme S1. Synthetic route of AVCOOEt.

2,4-Dinitrochlorobenzene (6.0 g, 30 mmol) and 4,4'-bipyridine (1.8 g, 12 mmol) were individually dissolved in ethanol (30 mL) and then mixed and refluxed for 72 h. A yellow powder precipitated, which was filtered and washed several times with hot ethanol and acetone to give 1,1'-bis-(2,4-dinitrophenyl)-4,4'-bipyridilium dichloride as a white powder.

1,1'-bis-(2,4-Dinitrophenyl)-4,4'-bipyridilium dichloride (0.84 g, 1.5 mmol) and ethyl 4-aminobenzoate (0.74 g, 4.5 mmol) were refluxed in ethanol (150 mL) for 48 h. The reaction mixture was cooled to room temperature, concentrated by rotary evaporation in vacuo to ca. 30 mL, and precipitated by adding excess ethyl acetate (150 mL). After standing for 1 h, the precipitate was collected by centrifugation. Recrystallization of this powder from methanol and THF, followed by drying in a vacuum-oven at 60 °C to obtain AVCOOEt as a faint yellow powder (0.63 g, yielded 80%). ^{1}H NMR (600 MHz, D_2O) δ (ppm) = 9.452 (d, J = 6.6 Hz, 4H), 8.822 (d, J = 6.0 Hz, 4H), 8.358 (d, J = 8.4 Hz, 4H), 7.954 (d, J = 8.4 Hz, 4H), 4.443 (d, J = 7.2 Hz, 4H), 1.397 (t, J = 7.2-14.4 Hz, 6H). ^{13}C NMR (150 MHz, D_2O) δ (ppm) = 167.23, 151.12, 145.62, 145.37, 133.37, 131.71, 127.35, 124.72, 63.00, 13.43.

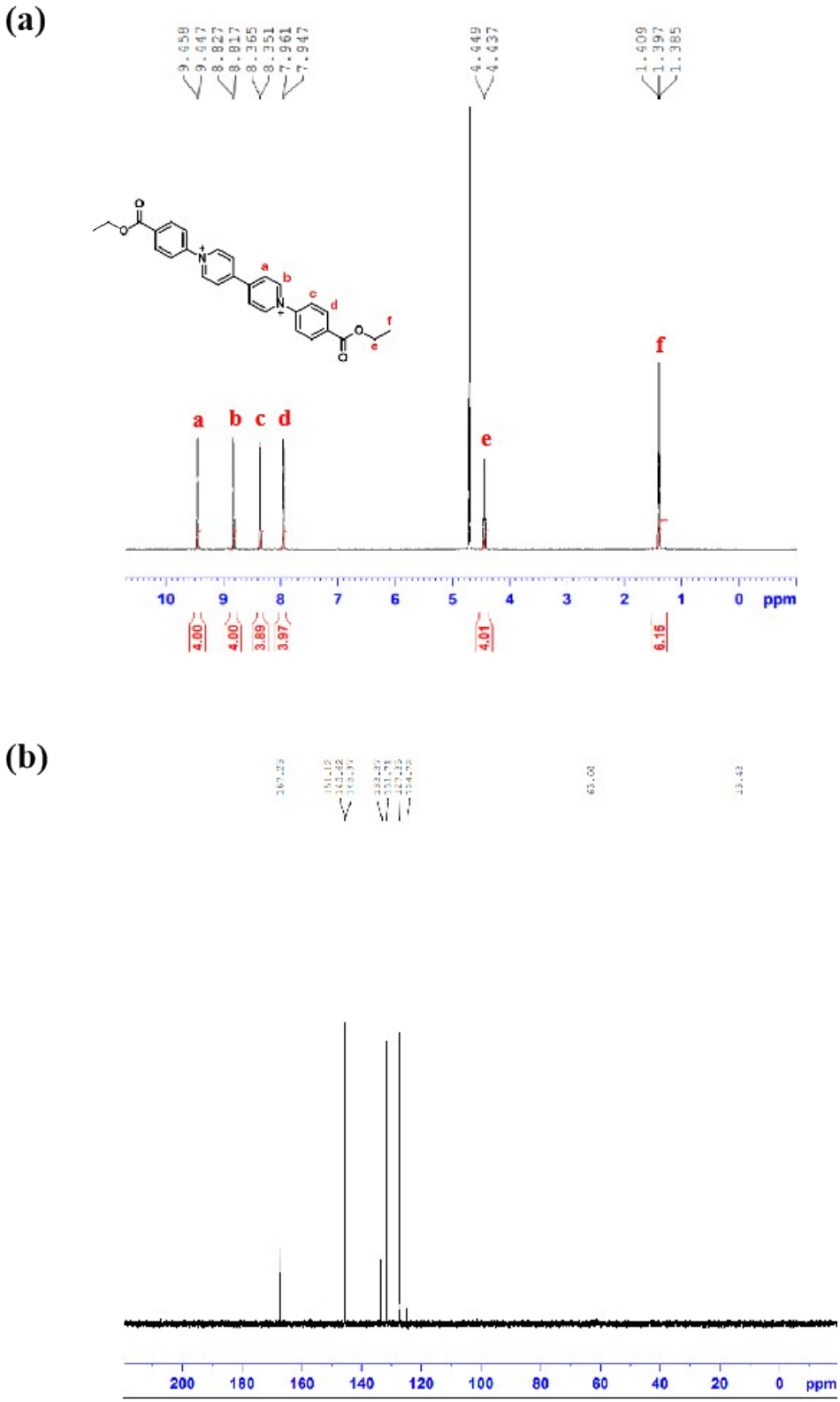

Fig. S1. ^{1}H NMR (a) and ^{13}C NMR (b) spectra of AVCOOEt.

S3. FT-IR spectra

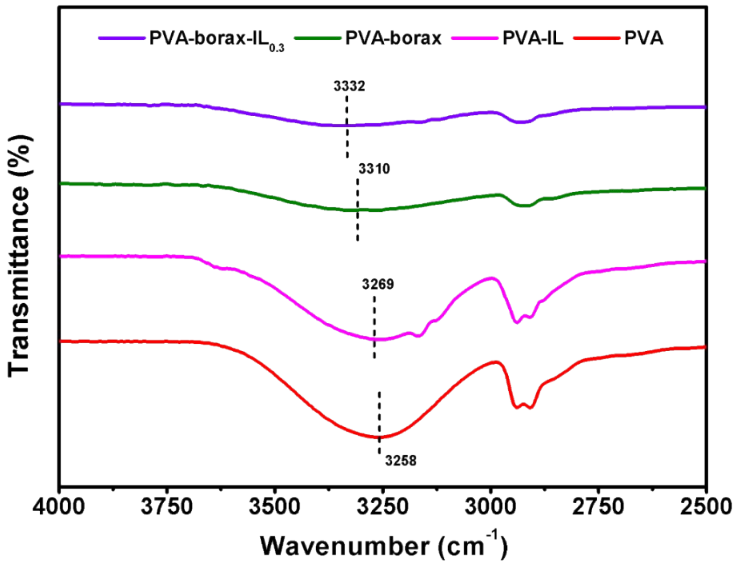

Fig. S2. FT-IR spectra of the freeze-dried PVA-borax-$IL_{0.3}$, PVA, PVA-IL, and PVA-borax in the region of 4000-2500 cm^{-1}.

S4. DSC curves

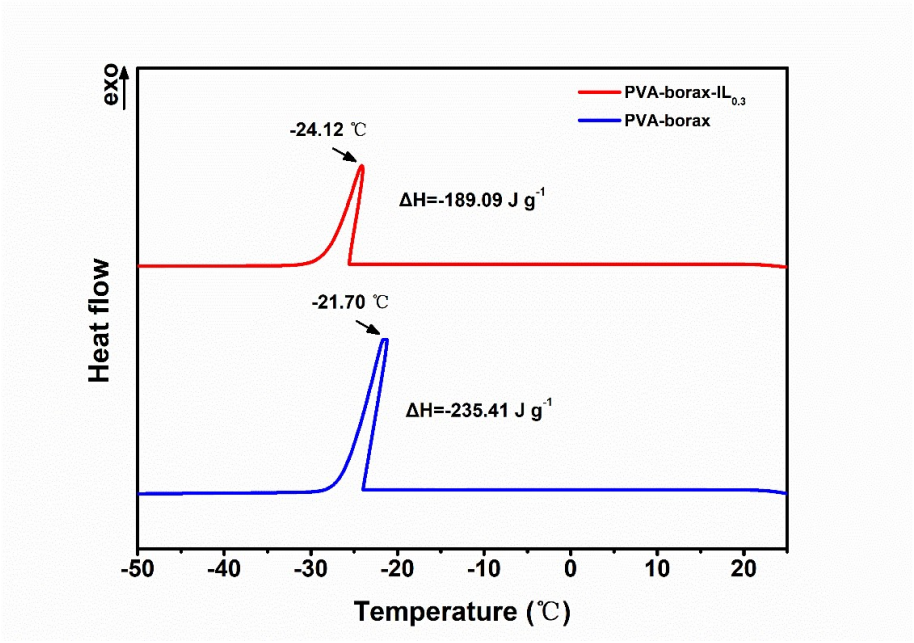

Fig. S3. DSC thermogram of the PVA-borax and PVA-borax-$IL_{0.3}$ HGEs at a cooling rate of 5 °C min^{-1}

S5. Photographs of HGEs

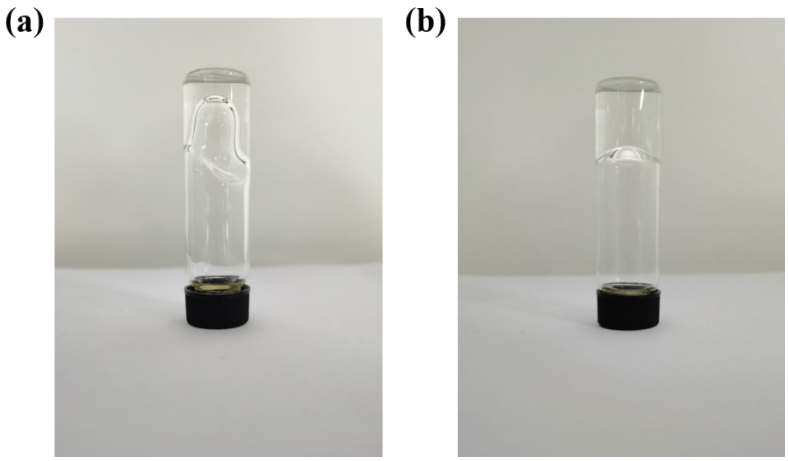

Fig. S4. Photographs of PVA_3-borax (a) and PVA_4-borax (b) HGEs.

S6. Ionic conductivity at higher IL concentrations

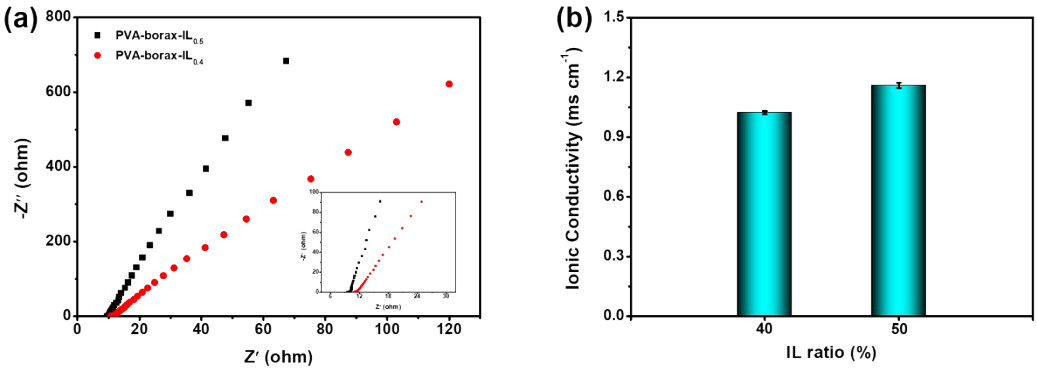

Fig. S5. Electrochemical impedance spectroscopy of the PVA-borax-IL HGEs with different IL concentrations (a) and their corresponding conductivities (b).

S7. Transparency image

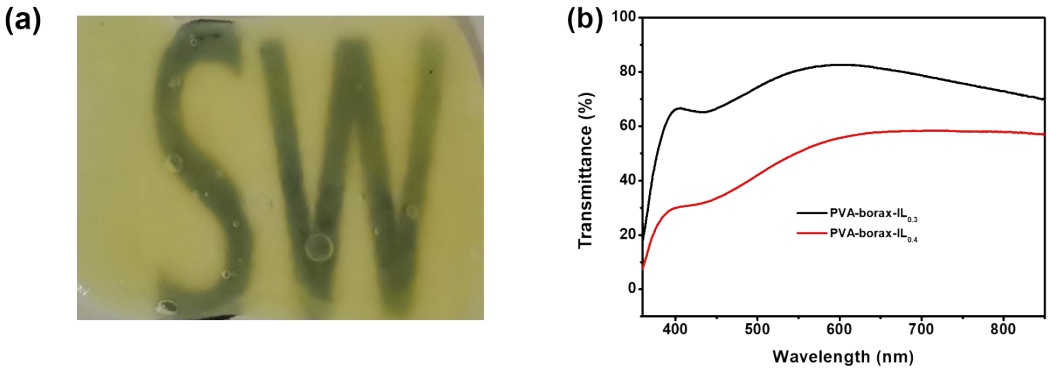

Fig. S6. Photographs of the PVA-borax-$IL_{0.4}$-AVCOOEt EC hydrogel (a). Optical transmittance spectra of the PVA-borax-IL-AVCOOEt with different IL contents (b).

S8. Electrochemical impedance spectroscopy

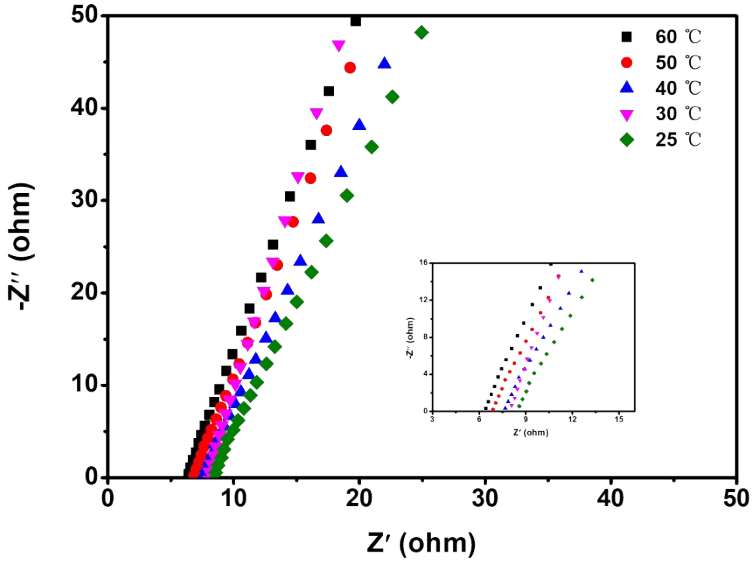

Fig. S7. Nyquist plots of the PVA-borax-$IL_{0.3}$ HGE at different temperatures from 25 to 60 ℃.

S9. Water decomposition voltage

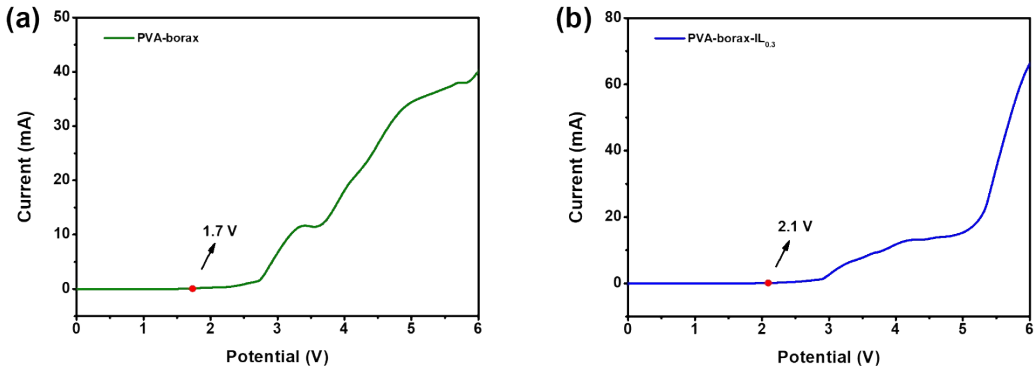

Fig. S8. Linear sweep voltammetry curves of the PVA-borax (a) and PVA-borax-$IL_{0.3}$ (b) HGEs.

S10. Dehydration curves

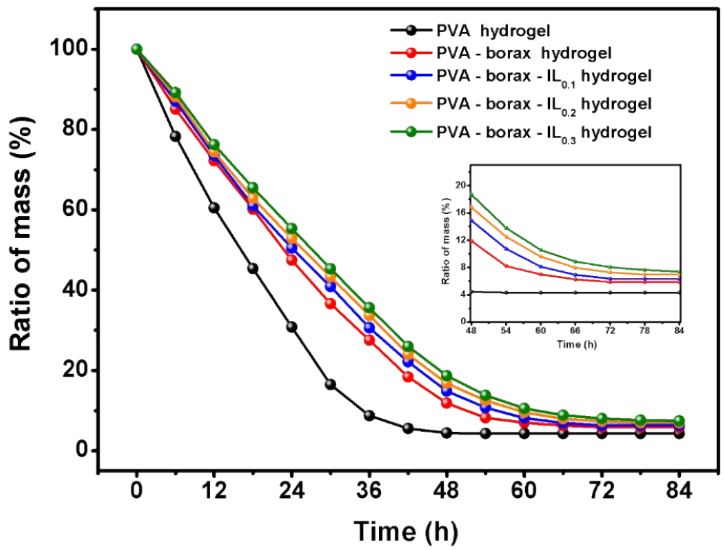

Fig. S9. Dehydration of PVA-borax-IL HGEs with varying borax and IL contents under 86% relative humidity at room temperature.

S11. Cyclic voltammograms of the ECD based on PVA-borax-$IL_{0.3}$-AVCOOEt

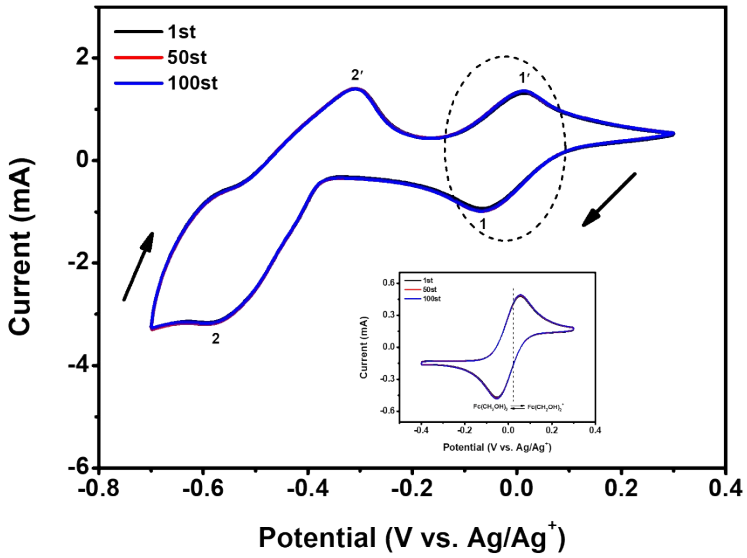

Fig. S10. Cyclic voltammetric diagrams of the ECD based on PVA-borax-$IL_{0.3}$-AVCOOEt EC hydrogel with 100 cycles at a scanning rate of 100 mV s^{-1} (vs. Ag/Ag^{+}). Insert: CV curves of $Fc(CH_2OH)_2$.

S12. Electrochromic behavior of the ECD based on PVA-borax-AVCOOEt EC hydrogel

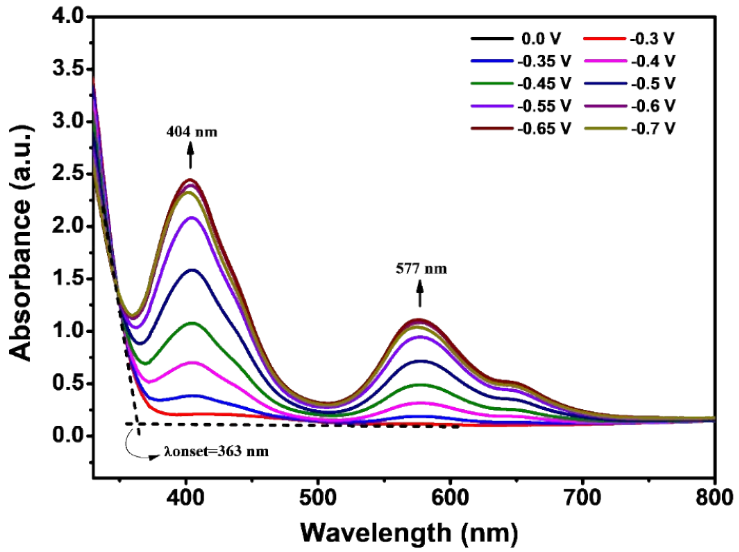

Fig. S11. UV–vis absorption spectra of the ECD based on PVA-borax-AVCOOEt EC hydrogel at different applied voltages.

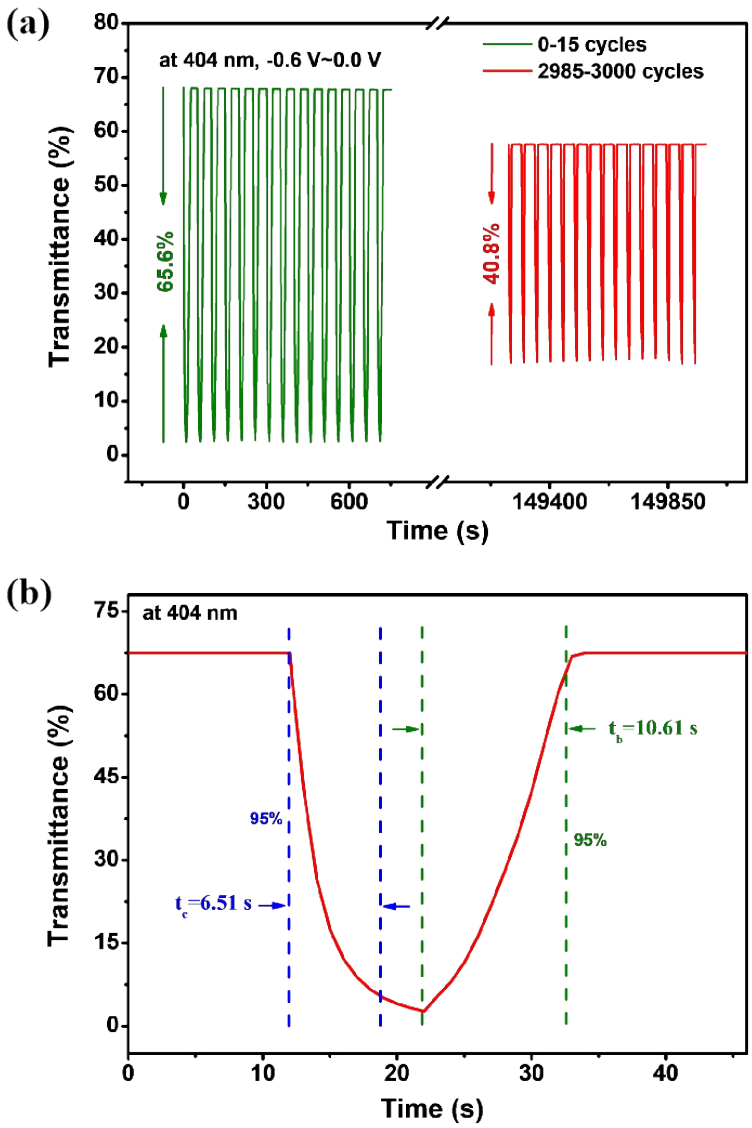

Fig. S12. Electrochromic switching response (a) and response time (b) of the ECD based on PVA-borax-AVCOOEt monitored at 404 nm between −0.6 and 0.0 V.

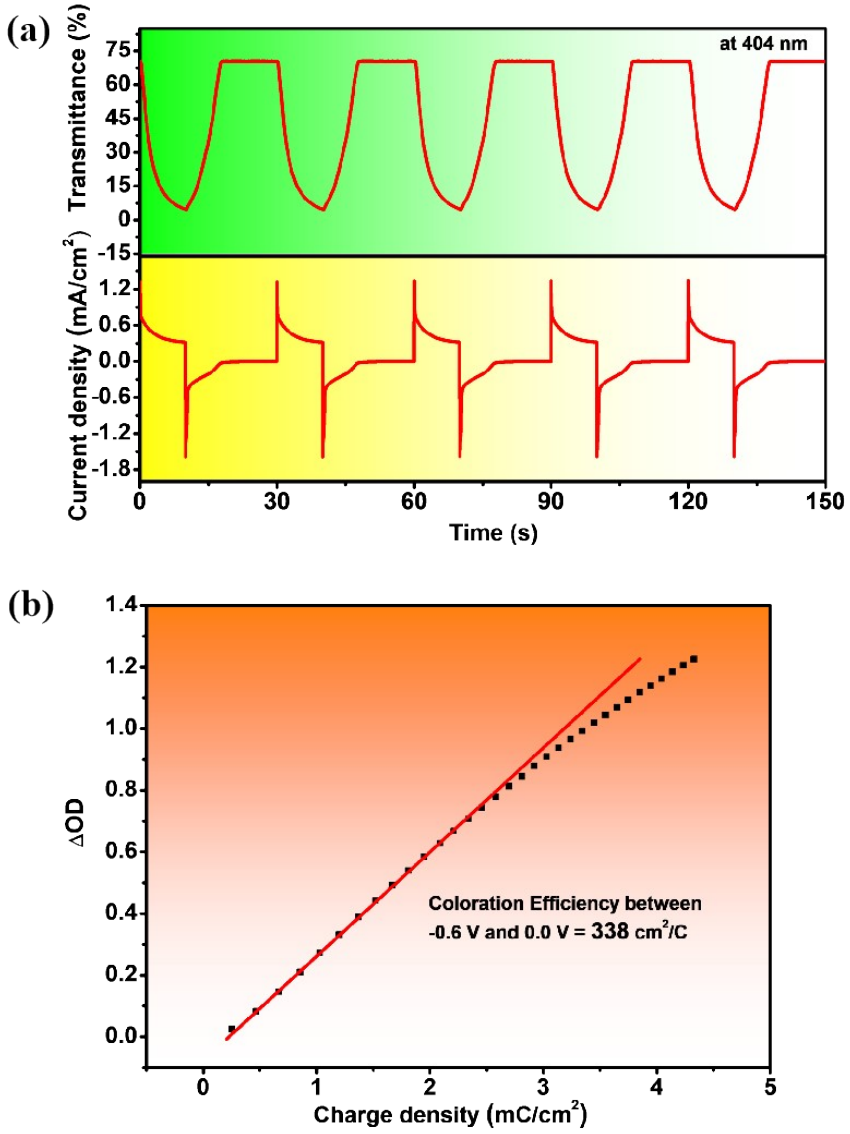

Fig. S13. Chronoamperometry curve and the corresponding in-situ transmittance curve (a) and optical density versus charge density (b) of the ECD based on PVA-borax-AVCOOEt at 404 nm between −0.6 V and 0.0 V.

S13. Memory behavior

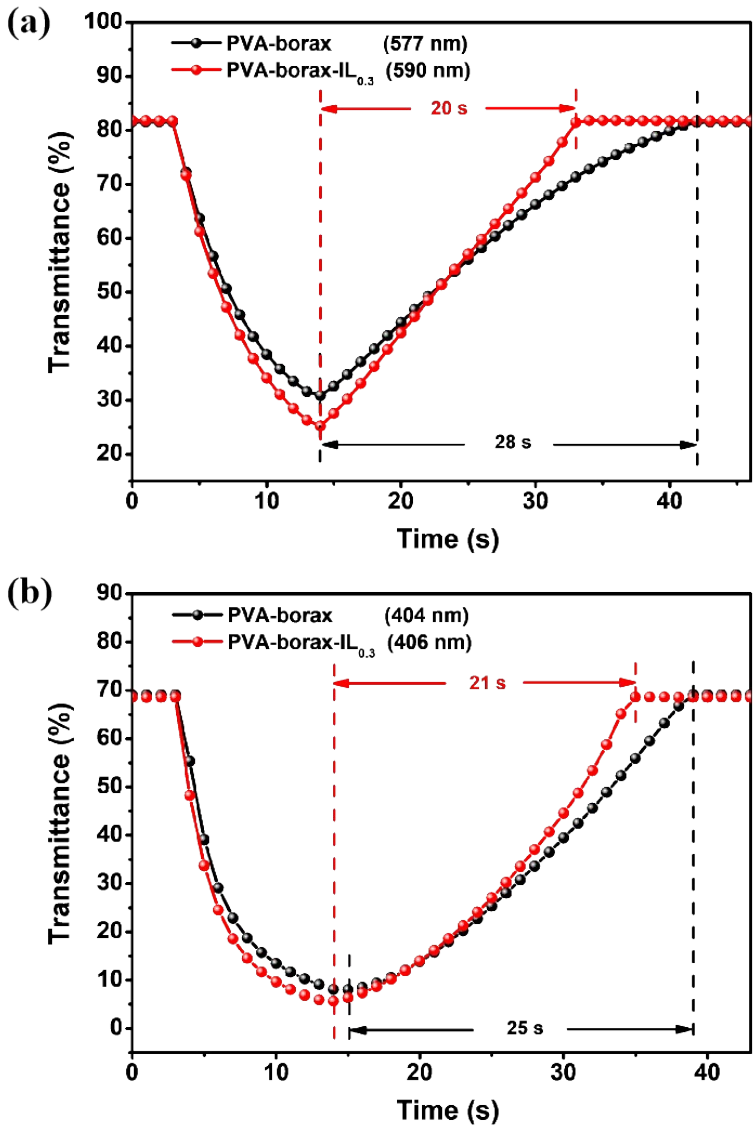

Fig. S14. Open-circuit memory of AVCOOEt-based hydrogel ECDs with PVA-borax and PVA-borax-$IL_{0.3}$ hydrogel electrolytes at (a) 404 and 406 nm, (b) 577 and 590 nm wavelengths, respectively, which are under open-circuit voltage.

S14. Transient distribution of current density and optical transmittance

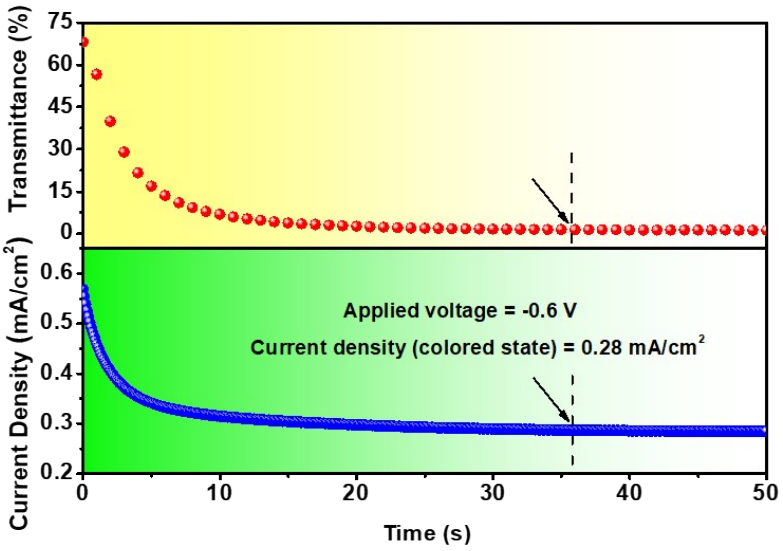

Fig. S15. Transient distribution of current density and optical transmittance of the ECD based on PVA-borax-$IL_{0.3}$-AVCOOEt upon application of −0.60 V at 406 nm.